Stabilization of Supramolecular Membrane Protein-Lipid Bilayer Assemblies Through Immobilization in a Crystalline Exoskeleton

Fabian C. Herbert,† § Sameera S. Abeyrathna,† § Nisansala S. Abeyrathna,† § Yalini H. Wijesundara,† Olivia R. Brohlin,† Francesco Carraro,§ Heinz Amenitsch,& Paolo Falcaro,§ Michael A. Luzuriaga,† Alejandra Durand-Silva,† Shashini D. Diwakara,† Ronald A. Smaldone,† Gabriele Meloni,† and Jeremiah J. Gassensmith*,†,‡*

†Department of Chemistry and Biochemistry, ‡Department of Bioengineering, The University of Texas at Dallas, 800 West Campbell Road, Richardson, TX 75080, USA §Institute of Physical and Theoretical Chemistry, Graz University of Technology, Stremayrgasse 9, Graz 8010, Austria. &Institute of Inorganic Chemistry, Graz University of Technology, Stremayrgasse 9, Graz 8010, Austria.

Abstract: Artificial native-like lipid bilayer systems constructed from phospholipids assembling into unilamellar liposomes allow the reconstitution of detergent-solubilized transmembrane proteins into supramolecular lipid-protein assemblies called proteoliposomes, which mimic cellular membranes. Stabilization of these complexes remains challenging because of their chemical composition, the hydrophobicity and structural instability of membrane proteins, and the lability of interactions between protein, detergent, and lipids within micelles and lipid bilayers. In this work we demonstrate that metastable lipid, protein-detergent, and protein-lipid supramolecular complexes can be successfully generated and immobilized within zeolitic-imidazole framework (ZIF) to enhance their stability against chemical and physical stressors. Upon immobilization in ZIF bio-composites, blank liposomes, and model transmembrane metal transporters in detergent micelles or embedded in proteoliposomes resist elevated temperatures, exposure to chemical denaturants, aging, and mechanical stresses. Extensive morphological and functional characterization of the assemblies upon exfoliation reveal that all these complexes encapsulated within the framework maintain their native morphology, structure, and activity, which is otherwise lost rapidly without immobilization.

Introduction

All living organisms, from prokaryotes to higher eukaryotes, rely on transmembrane protein systems for a variety of functions including signal transduction, substrate transport, and intramembrane enzymatic catalysis.[1] A significant fraction of polytopic transmembrane proteins act as transporters and are critical for the translocation of large and/or charged substrates in and out of the cell and understanding their function is imperative to understanding the etiology of many human diseases.[2-4] Purification of transmembrane proteins and subsequent reconstitution in artificial lipid bilayers—called proteoliposomes—generates metastable systems that are utilized for both structural analysis and functional investigations in which substrate transport can be studied on transporters embedded into their native–like environments.[5, 6] Unfortunately, owing to the patchwork of hydrophobic and hydrophilic surfaces of transmembrane proteins and the dynamic non-covalent nature of liposomes, these assemblies are intrinsically unstable and susceptible to denaturation, precipitation, and loss of function when left at room temperature for even a few hours. Despite years of effort toward stabilizing membrane-bound proteins, only a handful of approaches exist, and discovery of methods that protect them within their native bilayer environment remains an open challenge. Immobilization of biomacromolecular motion by chaperone-like confinement in polymers has emerged as a way to stabilize soluble proteins, but the accessibility of addressable functional groups of transmembrane proteins is reduced from confinement in a lipid matrix and the poor stability of membrane-bound proteins further complicates bioconjugation.[7] Recently,

polymeric excipients designed to match the natural distribution of polar residues on proteins[7] or stabilization in amphipathic copolymer-based membrane nanodiscs[8] have advanced the state-of-the-art; however, these coatings are neither removable nor scalable to protect a functional catalytic proteoliposome system. Specifically, a "sheddable" coating that avoids excipients or chemical functionalization of either protein or lipid would help advance work on these systems tremendously. To that end, we turned to metal-organic frameworks (MOFs), which are a class of crystalline porous coordination polymers constructed from the interlinking between metal centers and monomeric organic ligands.[9-11] Through thoughtful selection of the organic ligand and metal center, MOFs can be modulated sophisticatedly towards a wide array of applications[12] such as gas separation/sensing/storage,[13-15] catalysis,[16-18] and protein stabilization.[19-21] In recent years, several MOFs displaying zeolitic topologies have been reported,[22] the most ubiquitous being zeolitic-imidazole framework-8 (ZIF-8) and associated structural analogues, all of which are coordination polymers consisting of Zn^{2+} and 2-methyl imidazole (MIM).[23,24] ZIF-8 and its associated (pseudo)polymorphs can form thermodynamically stable crystalline shells by nucleating on biomacromolecules[25] and these systems can withstand high temperatures and pH[26] yet are kinetically labile in the presence of metal binding chelates.[27-29] ZIF-8 in particular is well known for its ability to nucleate on the surface of colloidal and dissolved biomacromolecules forming a crystalline matrix shell.[30,31] We suspected that colloidal liposomes, proteoliposomes, and detergent solubilized transmembrane proteins would nucleate the growth of ZIFs over their surface, and this protective shell would inhibit both protein denaturation and liposome fusion and/or degradation. Further, the kinetic lability of Zn-MIM bond in the presence of high-affinity metal chelators would allow us to recover the encapsulated systems without significant loss of protein function or sample homogeneity.

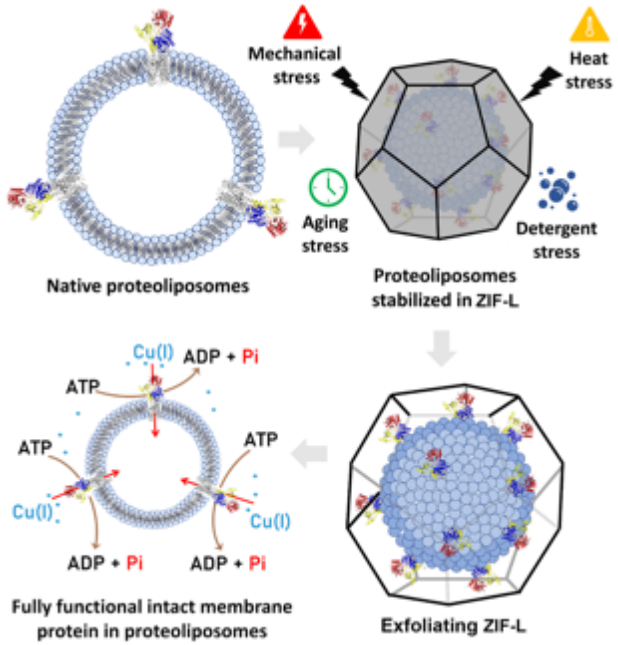

Scheme 1. Proteoliposome stabilization through biomolecular nucleation in ZIF-L. The scheme portrays the process by which the proteoliposome after encapsulation can resist different forms of stress. An 'exfoliating step' is then used to remove the shell and free the proteoliposomes when ready for analysis. Even after intense stressing, catalytic activity of transmembrane copper transporters remains very high.

In this study, we demonstrate a method for the thermal stabilization of (i) blank 200 nm liposomes, (ii) purified transmembrane proteins, and (iii) 200 nm transmembrane protein-liposome supramolecular complexes (proteoliposomes) against chemical and thermal stressors through biomimetic nucleation of a pseudopolymorph of ZIF-8 called ZIF-L. We selected two α-helical polytopic (8 transmembrane α-helices) iron and copper transporters—called IroT/MavN and CopA respectively— as representative examples of metal transport systems and virulence factors in bacteria that cause fatal human diseases.[32, 33] Transition metal transporter proteins are the subject of ongoing research in a number of laboratories,[34-36] and their stabilization serve not only as a proof-of-concept but also in aiding research into these systems. We found that encapsulation of the proteoliposome complex generates thermodynamically stable bio-composites that can withstand exposure to high temperatures, aging, and common protein denaturants (**Scheme 1**). Further, the ZIF-L coatings can be removed to afford pristine proteoliposomes, liposomes, and transmembrane protein micelle complexes of similar composition, morphology, structure, and catalytic activity to their native counterparts. Finally, our work demonstrates the generalizability and potential ZIF scaffolds have for stabilizing highly sensitive and metastable supramolecular systems.

Results and Discussion

Liposome Stabilization

We progressed systematically to demonstrate that each component—the as-prepared liposome, the detergent purified protein, and the proteoliposome system—could be encapsulated and protected by biomolecular nucleation. We prepared 200 nm liposomes by freeze-fracture and extrusion using mixtures of L-α-phosphatidylcholine and *E. coli* total polar lipid extracts, that allow the formation of native-like unilamellar lipid bilayers. While this composition was selected because it provides the best stabilization for our selected transmembrane proteins, the anionic nature of the formulated lipids are useful in promoting ZIF nucleation and growth, as we and others have demonstrated.[37,38] Prior work with ZIF-8 synthesis has been done in pure water; however, the internal composition of the liposome lumen requires ideal buffering conditions to guarantee protein activity and stability when the proteoliposomes are generated and avoid osmotic bursting. Instead, we used a solution of 100 mM NaCl, 1 mM TCEP, and 20 mM MOPS buffered to a pH of 7.0 (M-buffer) as a solvent and systematically varied the concentrations of Zn salt and MIM until liposomes (Lp) were quantitatively captured within ZIF-L shells forming Lp@ZIF (**Figure 1A**).

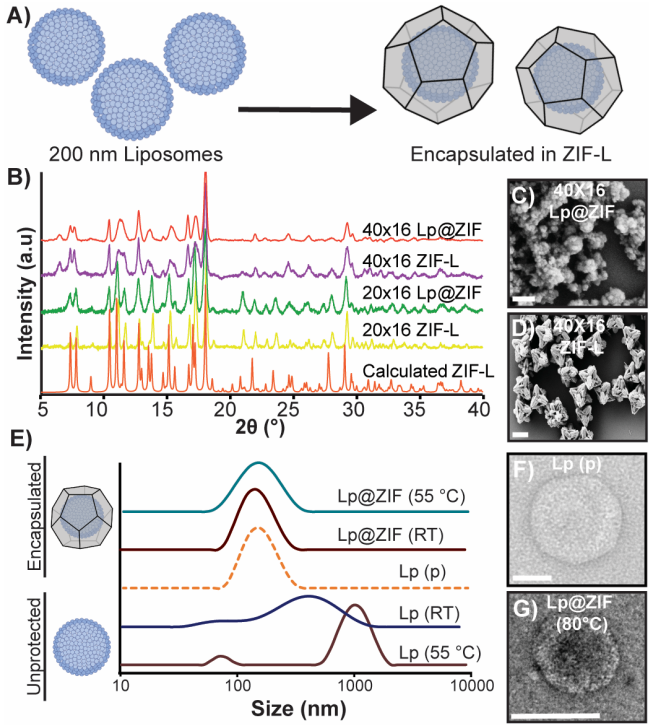

Figure 1. Characterization of artificial lipid bilayers embedded in ZIF. A) Biomolecular nucleation of liposomes in ZIF. B) PXRD spectra of ZIF liposome complexes (Lp@ZIF) and ZIF controls. SEM micrograph of C) 40×16 Lp@ZIF (Scale bar = 200 nm) and D) 40×16 pristine ZIF (Scale bar = 2µm). E) DLS profiles obtained for immobilized liposomes exposed at high temperatures (after exfoliation) compared to native and non-encapsulated liposomes. F) TEM micrograph of pristine liposome (Scale bar = 50 nm) and G) 40×16 Lp@ZIF following exfoliation after exposure to 80 °C for 5 min (Scale bar = 100 nm).

Our investigation focused primarily on two synthetic conditions that produced crystal encapsulated liposomes—M-buffer and 20 mM of zinc acetate dihydrate and 320 mM MIM, which is an MIM concentration 16-fold higher than the metal concentration (20×16) and 40 mM of $Zn(OAc)_2$ with 640 mM MIM (40×16). Precursor solutions of zinc acetate dihydrate, MIM, and 200 nm liposomes were mixed to immediately yield a white flocculate. Crystal were allowed to age at RT for 18 h, then the artificial lipid bilayer-embedded ZIF crystals were harvested by centrifugation, washed, and allowed to dry at RT for 12 h. Encapsulation efficiency was determined by fluorescence. Cyanine-5 (Cy5, $\lambda_{Ex=}$ 651 nm and λ_{Em}= 670 nm) was entrapped within the liposomal lumen during liposome extrusion. After washing, the fluorescent liposomes were encapsulated using both the 20×16 and 40×16 conditions (**Figure S1**). The supernatants from the reactions were collected and from the residual fluorescence we determined encapsulation efficiency, where we found that both conditions afforded high liposome loading (90%). Fluorescence imaging, Powder X-Ray diffraction (PXRD) and Scanning Electron Microscopy (SEM) analysis of the Lp@ZIF formulation as well as controls were carried out (**Figures 1 B-D and Figures S1 and S2**). Intrigingly, XRD patterns obtained for both conditions, including controls, are consistent with the formation of ZIF-L, a crystalline phase with a leaf-like morphology that explains the highly faceted nanoparticles observed in the micrographs in **Figures 1 C & D**.[39] Nitrogen isotherms of both liposome loaded composites and controls reveal low porosity (**Figure S2 C and Table S1)**, which is consistent with ZIF-L.[40] Finally, thermogravimetric analysis (TGA) of 20×16 Lp@ZIF and 40×16

Lp@ZIF both display a mass loss (~18%) at 200 °C, which has been attributed to solvent loss in prior work with ZIF-L (**Figure S2 D**).[41]

The protective capacity of the ZIF-L coating toward the liposomes was evaluated on samples suspended in water and stressed at RT for 48 h and 55 °C for 15 min—this latter temperature being above the phase transition temperature of the liposomes. After stressing, the ZIF-L shell was dissolved in ethylenediaminetetraacetic acid-EDTA- (50 mM)—a process we refer to as exfoliation (**Scheme 1**)—and these solutions were analyzed by dynamic light scattering (DLS) to assess liposomal size distribution. As controls, we stressed non-encapsulated liposomes following the same experimental conditions. As expected, the unprotected liposomes showed a significant increase in size and polydispersity (average diameter: 604.8 nm; PDI: 0.449; **Table S2**) resulting from membrane fusion and liposome aggregation (**Figure 1 E, lower two traces**) under both conditions. Conversely, we were happy to find that the monodisperse nature of freshly extruded blank liposomes (average diameter: 141.2 nm; PDI: 0.138) was retained for the ZIF-L coated composites (average diameter: 123.2 nm; PDI: 0.179; **Figure 1 E top two traces**). Preservation of the original liposomal morphology in ZIF-L immobilized samples was further confirmed by transmission-electron microscopy (TEM, **Figure 1 F-G**). While the stressed ZIF-L liposomes showed liposomes that were indistinguishable from freshly extruded pristine samples, unprotected liposomes showed altered morphology as a consequence of extensive membrane rupture and fusion (**Figures S3)**. In light of the observed stabilization, Lp@ZIF composites were thermally stressed at 80 °C and subsequent analysis by DLS and TEM imaging revealed that the original morphology and size distribution was largely retained (average diameter: 119.3 nm; PDI: 0.231; **Figures S4**). To test the ability of ZIF encapsulation in protecting from aging, Lp@ZIF was dried and the obtained hydrated suspension left on the benchtop for 20 days at room temperature. Following exfoliation, TEM characterization revealed that the liposomes retained their original size distribution and morphology (**Figures S3 and S4**). In contrast, the non-encapsulated liposomes kept in solution fused and/or aggregated within two days (**Figures S3 F-I**). Interestingly, both formulations discussed above (20×16 and 40×16) provided outstanding protection against thermal stress and aging following liposome immobilization in ZIF-L composites (**Figures 1, S3 and S4**).

Finally, we and others have previously reported that different polymorphs of ZIF can be produced by increasing the concentration of ligand and metal.[22,30] This is potentially useful as different polymorphs can impart greater or less protection and the kinetics of dissolution can be very different, which may be useful in drug delivery applications. We were able to find conditions that resulted in the growth of the ZIF-8 sod topology (**Figure S5**). Though, qualitatively, we noticed it was more time consuming to exfoliate the ZIF-8 polymorph as compared to ZIF-L. That said, we found we could recover the liposomes intact (**Figure S6**). Further study is underway to fully evaluate the relative levels of protection afforded by the different polymorphs of ZIF and the kinetics of their exfoliation; however, the ZIF-L composites provided outstanding protection and were used throughout the work.

Mechanism of ZIF Growth

In reactions with ZIF and its associated polymorphs, we and others have observed that the initial interaction occurs between the biomolecule surface and the zinc ions and this interaction has been proposed as an important indicator for a biomimetic crystallization process on the surface of biomacromolecules.[26,30,83] We were able to confirm qualitatively that zinc can bind to the negative surface of liposomes, which have a −16.9 mV ζ potential (**Figure S7 A and B**) from the presence of anionic phospholipids, by observing zinc-lipid complexes by inductive coupled plasma mass spectrometry (ICPMS). When the lipids were doped with 1,2-dioleoyl-3-trimethylammonium propane (DOTAP), a cationic lipid, we observed less or even no Zn^{2+} interaction with the liposome (**Figure S7 C and D**). Cationic surface charge has been shown to reduce the encapsulation yield or even prevent crystal growth, although there are strategies to overcome this, and we are actively studying this. Kinetics of nucleation, particle growth,[38] crystallization, and the morphology of the particles were investigated *in situ* via synchrotron-based small-angle and wide-angle X-ray scattering (SAXS/WAXS) techniques.[42,43] We investigated four different samples (20×16 Lp@ZIF, 20×16 ZIF-L, 40×16 Lp@ZIF, and 40×16 ZIF-L) using a stopped flow device to initiate the rapid mixing

of the reagents (mixing time <100 ms). See the SAXS section of the SI for full experimental details. The injection of the aqueous precursors solutions (Zn^{2+}, MIM, liposomes) into a micromixer triggered the SAXS acquisition system data collection (time resolution: 100 ms). Data for the 20×16 conditions are summarized in **Figure 2** below—see the SI for 40×16 results. To investigate the kinetics of nucleation and growth, we monitored the time evolution of SAXS patterns (**Figures 2 A & B**) and of the invariant Q̃ (**Figure 2 C**, see ESI for details).[41] Q̃ is related to the Porod invariant of the scattering curve and is sensitive to changes in particle volume fraction and electron density contrast. An increase of Q̃ over time indicates the formation of particles/agglomerates within the investigated volume of the sample. A plateau in the time series of Q̃ values indicates stationary conditions. The time evolution of Q̃ is reported in **Figure 2C** and in the "Time-resolved Small Angle X-Ray Scattering (SAXS)" section of the Supporting Information. The increase of Q̃ related to the particle growth is observed 0.8 s and 0.6 s after the mixing of precursors for samples 20×16 Lp@ZIF and 40×16 Lp@ZIF, respectively. In the control samples, the particle growth is observed 4 s (20×16 ZIF-L) and 2.6 s (40×16 ZIF-L) after mixing the precursors. The plateau of Q̃ related is reached 25 s and 5 s after the mixing of precursors for samples 20×16 Lp@ZIF and 40×16 Lp@ZIF, respectively. In the control samples, the plateau is reached 40 s (20×16 ZIF) and 25 s (40×16 ZIF) after mixing the MOF precursors.

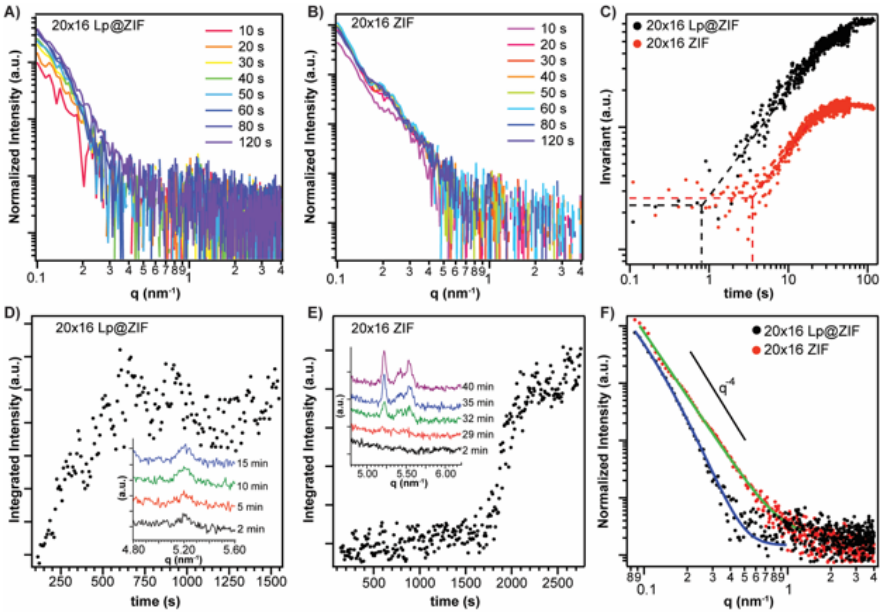

Figure 2: Time evolution of SAXS patterns (background subtracted) from time-resolved SAXS synthesis of A) 20×16 Lp@ZIF and B) 20×16 ZIF measured at 10 s intervals. C) Time evolution of invariant Q̃ calculated from 0.1 – 0.6 nm^{-1} of the time-resolved SAXS patterns in panels A and B and corresponding to the synthesis of 20×16 Lp@ZIF (black dots) and 20×16 ZIF-L (red dots). The dashed lines are plotted to highlight the starting time of the Q̃ increase. D) Time evolution of the integrated intensity of (200) diffraction peak of ZIF-L (5.25 nm^{-1}) calculated from time-resolved SAXS synthesis 20×16 Lp@ZIF and E) 20×16 ZIF-L. In the insets, selected diffraction patterns highlighting the time-evolution of the (200) diffraction peak of ZIF-L (5.25 nm−1) are reported. Time zero is referred to the end of the precursors mixing. F) SAXS patterns (background subtracted and averaged) and fitted data 120 seconds after mixing the precursors of 20×16 Lp@ZIF (black dots) and 20×16 ZIF-L (red dots). The theoretical Porod power law ($I(q) \propto q^{-4}$) is plotted for comparison.

The crystallization kinetics were monitored by following the integrated intensity of the (200) ZIF-L diffraction peak (5.25 nm^{-1}; **Figures 2 D & E**). In the presence of liposome, the added mixture of Zn and MIM initially produced an amorphous phase for both the 20×16 and 40×16 conditions between 0.1–120 s and 0.1–50 s respectively. The initial formation of an amorphous phase is consistent with what we have observed with viral nanoparticles and other proteins.[30,42,44] Importantly, compared to the control samples, we observed faster crystallization for Lp@ZIF particles (*e.g.* 20×16 Lp@ZIF crystallization is 15 times faster than the pure ZIF-L particles; **Figures S16–S19**). These data demonstrate that the presence of liposomes templates a faster nucleation, growth, and crystallization of ZIF-L when compared with the control conditions.

By fitting the SAXS patterns 120 seconds after the mixing of the reagents (**Figure 2 F**), we observed that the presence of the liposome induced the formation of plate-like particles with a thickness of 30–50 nm. Conversely, in the absence of liposomes, ZIF particles with an average size larger than 100 nm and no sharp size distribution were observed. Thus, a role of the biomacromolecules in the final crystal morphology was determined.[26] From these data,

we conclude that the liposomes act as seeding agents for the MOF growth, altering their growth kinetics as well as the ultimate morphology of the crystalline particles that are produced and that liposome MOF biocomposites are formed via a biomimetic mineralization process.[43,45]

Stabilization of Purified Transmembrane Proteins

We selected two different transmembrane proteins, both of which are poorly stable at room temperature, to demonstrate the broad utility of our approach. IroT/MavN is a transmembrane protein found in *Legionella pneumophila* (*L. pneumophila*), a thin, flagellated, gram-negative bacteria responsible for Legionnaires' disease.[46] IroT meditates iron sequestration as an essential micronutrient from host cell, allowing for *L. pneumophila* to replicate in a host-derived vacuole within the infected macrophages.[47] IroT topology is characterized by 8 transmembrane (TM) helices and a long C-terminal domain.[48, 49] The structure and substrate translocation modality in IroT are active areas of research, but much has been gleaned from reconstituting IroT in artificial lipid bilayer systems and performing real-time transport assays.[49] IroT was shown to act as a Fe^{2+}/H^{+} antiporter that allows Fe^{2+} acquisition into the vacuole from the host cell for pathogen survival.[48] The second protein selected is a copper P_{1B}-type ATPase from *E. coli* (CopA), a transmembrane primary-active pump, and part of the P-type ATPase superfamily, that utilize energy generated by ATP hydrolysis to drive Cu^{+} transport across biological membranes against electrochemical gradients.[50,51] These catalytically driven pumps constitute an essential system to drive the selective translocation and export of Cu^{+} ions, thereby controlling the intracellular Cu^{+} levels.[52,53] Their activity tightly balances the biogenesis and integrity of copper centers in vital enzymes to non-toxic intracellular copper levels. The CopA structure is characterized by the existence of an 8 TM helices membrane domain (M-domain) connected to large cytosolic domains (N-, P- and A-domains) responsible for ATP hydrolysis, phosphorylation and energy transduction, allowing Cu^{+} translocation across the membrane.[35, 50, 52, 54] As a result of their critical involvement in essential iron and copper metabolism, both IroT and CopA homologues have been identified as key virulence factors in bacterial pathogens.[37,55]

Transmembrane proteins, including IroT and CopA, are commonly extracted from membranes and purified as detergent micellar complexes for solubilization in aqueous environments. The detergent molecules surround the hydrophobic regions of the protein in the micelles, which helps avoid aggregation, precipitation, and refolding in water. Though they are more stable, these proteinaceous assemblies still require unique environmental conditions to remain fully active—*e.g*. long-term storage at −80 °C, constant refrigeration for analysis *etc*. Since this strategy is employed in the typical workflow for incorporating transmembrane proteins in liposomes,[39,47] and naked transmembrane proteins are extremely prone to denaturation, we suspected simply nucleating the ZIF over the detergent-protein supramolecular complex would improve the likelihood of retaining protein function in high yields following exfoliation. We thus solubilized and purified IroT as in Cymal-7 (7-Cyclohexyl-1-Heptyl-β-D-Maltoside) micelles and CopA in micelles prepared with DDM (*n*-Dodecyl-β-D-Maltopyranoside) and applied our synthetic strategy, developed above, to produce ZIF-L composites (**Figure 3A**). Crystals were isolated by centrifugation, washed, and allowed to dry at RT for 12 h. As-obtained crystals were characterized by SEM and showed a star-shaped morphology (**Figures 3 B-E and Figures S8 A and B**) and PXRD of both protein-micelle composites and controls again showed the phases to be ZIF-L (**Figure 3 F**)**.** TGA analysis of 40×16 IroT@ZIF and 40×16 control revealed high thermal stability as shown in **Figure S8**, where the 40×16 IroT@ZIF is characterized by an ~20% mass loss at 200 °C, attributed to loss of solvent (**Figure S8 C**).[41] Further, nitrogen isotherms of 40×16 IroT@ZIF reveal no measurable porosity, whereas 40×16 ZIF-L shows a BET surface of 385 m^2g^{-1} (**Table 1**).

Quantification of encapsulation efficiency was determined by SDS-PAGE gel densitometry. Supernatants obtained during the washing of ZIF-L bio-composites and exfoliated protein-detergent complexes were run in tandem with either IroT or CopA pristine standards of varying concentrations. We found the encapsulation efficiency to be quantitative—no residual protein was found in the supernatant after the encapsulation procedure. Indeed, after encapsulation, isolation of the final protein@ZIF product, and subsequent exfoliation, resulted in almost 75% recovery, regardless of the protein or metal-to ligand ratio used (**Figure S9 A–C**).

To determine the integrity of IroT or CopA detergent-protein micelles after biomolecular nucleation, two properties were analyzed to benchmark the protective effect of immobilization: i) monodispersity analysis by size-exclusion chromatography (SEC) for IroT; and ii) catalytic metal transport activity assessed by metal-stimulated ATP-hydrolysis, for CopA. SEC is a good proxy for testing the stability of the generated IroT-detergent complexes as the absence of aggregation is an indicator of the integrity and stability of the protein-detergent assembly. On the other hand, for purified Cu^{+} P-type ATPases, we can measure the rate of ATP hydrolysis in the presence of selected metal substrate to show persistence of structure and function, as ATP hydrolysis and Cu^{+} transport in CopA are tightly coupled. To verify CopA functionality in detergent micelles (or upon incorporation in proteoliposomes) the Cu^{+}-dependent stimulation of ATPase activity was determined by photometric quantification of released inorganic phosphate (P_i) generated by catalytic ATP-hydrolysis using Malachite green. Upon stressing, immobilized samples were exfoliated and immediately characterized by either SEC or metal-dependent ATP-hydrolysis assays. The non-encapsulated IroT samples showed increased polydispersity when incubated at RT, as evidenced by development of an asymmetric elution peak shoulder in SEC and almost complete aggregation after exposure to 55 °C and 80 °C for a few minutes (**Figures 3 G, S10 A**). This is to be expected, as these proteins are extremely prone to aggregation at even low temperature. In contrast, for the encapsulated samples, exposure to RT for 48 h and 55 °C for 15 min had little impact on the monodispersity of IroT. SEC analysis of the exfoliated IroT samples show a single elution peak (elution volume = 12.0 mL), closely corresponding to non-stressed and refrigerated IroT controls (12.0 mL) as shown in **Figure 3 G**. Incredibly, even exposure to 80 °C (5 min) produced minimal aggregation (**Figure S10 A**).

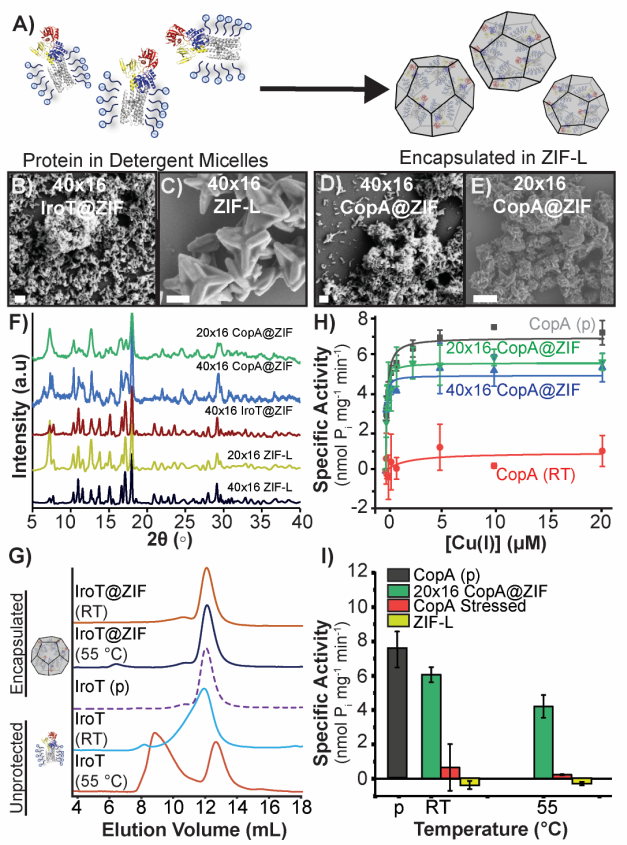

Figure 3. IroT@ZIF and CopA@ZIF characterization. A) Biomolecular nucleation of detergent stabilized CopA and IroT in ZIF. SEM micrographs of B) 40×16 IroT@ZIF (Scale bar = 200 nm) and C) 40×16 ZIF-L (Scale bar = 1μm). SEM micrographs of D) 40×16 CopA@ZIF (Scale bar = 200 nm) and E) 20×16 CopA@ZIF (Scale bar = 1μm). F) PXRD of 40×16 IroT@ZIF, 40×16 CopA@ZIF , 20×16 CopA@ZIF , 20×16 ZIF-L, and 40×16 ZIF-L. G) SEC traces of heated IroT@ZIF bio-composites against native and non-encapsulated IroT. H) ATPase activity analysis of CopA after stressing and exfoliation with unencapsulated control (red line). I) Comparison of maximal specific activity in CopA samples and controls.

Resilience to thermal stress was subsequently investigated on the CopA-DDM micelle complexes by analyzing the catalytic substrate-dependent ATP hydrolytic activity after exposing the various samples suspended in water to a range of denaturing temperatures. Cu^{+}-dependent stimulation of ATPase rates for non-stressed CopA, in the presence of Mg^{2+}/ATP, revealed characteristic catalytic hyperbolic Michaelis–Menten-type dependency as a function of Cu^{+}, confirming that the purification in detergent micelles maintains CopA in a functional form ($K_{M,\,Cu(I)} = 0.12 \pm 0.02$ μM; V_{max} of 7.1 ± 0.2 nmol (mg·min)$^{-1}$). However, upon thermal stress at RT, 55 °C and 80 °C, the CopA-DDM catalytic activity was completely abolished, with < 10% residual activity at RT. In contrast to unprotected protein, stressed samples of CopA encapsulated in ZIF retained the characteristic Michaelis-Menten dependency of

their ATPase activity after thermal stress and exfoliation (**Figure 3 H**). Analysis of CopA@ZIF bio-composite ATPase activities at saturating Cu^{+} concentrations revealed that CopA retained > 80 % (6.3 nmol P_i mg^{-1} min^{-1}) of its maximal ATPase activity upon stress at RT (**Figure 3 I**), > 60% at 55 °C (4.7 nmol P_i mg^{-1} min^{-1}; **Figure 3 I**) and at > 42% at 80 °C (3.1 nmol P_i mg^{-1} min^{-1}; **Figure S9 D**). Accordingly, analysis of the $K_{M, Cu(I)}$ values at RT indicated that upon stress unaltered catalytic parameters are preserved by ZIF encapsulation **(Figure S9 E).**

It is noteworthy that formulation conditions are an important aspect of stability. CopA was encapsulated under both metal-to-ligand ratios discussed above (20×16 and 40×16) and, interestingly, IroT-cymal-7 micelles showed better stabilization with the 40×16 formulation, while the 20×16 formulation was most effective at enhancing the thermal stability of CopA-DDM micelles. Thus, formulation optimization is an important parameter to be screened for optimal bio-composite protection depending on the protein topology and protein-detergent micelle structure **(Figure S9 D–F).**

Encapsulation of proteinaceous materials has been widely used to increase stability of moieties against chemical stressors, such as organic solvents and chaotropic agents.[33,34] Motivated by such reports, CopA@ZIF and IroT@ZIF were chemically stressed using SDS, a commonly used protein denaturant. Briefly, the samples were incubated for 30 min in a solution consisting of 0.1% SDS. Crystals were harvested by centrifugation, washed 5× with ultra-pure water, exfoliated, and immediately characterized by SEC analysis (IroT) or Cu^{+}-dependent ATP-hydrolysis assays (CopA). As shown in **Figure S10 C** & **D**, immobilization in ZIF affords retention of monodispersity and activity for both encapsulated transmembrane proteins, while non-encapsulated control samples are fully denatured and inactive in the presence of 0.1% SDS. These results also suggest that a population of proteins are at least partly exposed to the MOF surface, accounting for the modest (~15 %) loss of functionality. [36]

Proteoliposome Stabilization

Our analysis demonstrates that immobilization in new ZIF composites allow for stabilization of both pristine liposomal vesicles as well as protein-detergent micellar complexes, providing a 3D scaffold that can morph around complex and chemically diverse biomolecular assemblies providing protection against stressors. In light of the versatility of the approach, we sought to determine if our ZIF encapsulation strategy could protect even more complex and metastable supramolecular entities such as proteoliposomes. Purified IroT and CopA were reconstituted in unilamellar liposomes via freeze−thaw and extrusion through 200 nm filters, followed by liposome destabilization by detergent addition and subsequent detergent removal by Biobeads resin. Protein incorporation was subsequently quantified by SDS-PAGE following removal of excess detergent solubilized protein from the proteoliposomes by ultracentrifugation with subsequent protein quantification of the soluble and proteoliposome fractions conducted by gel densitometry. We subsequently biomimetically mineralized proteoliposomes with IroT or CopA embedded in the lipid bilayer in ZIF (**Figures 4 A-C and S11-12**). In a typical experiment, 6.25 mg mL^{-1} of proteoliposomes (protein concentration is 0.25 mg mL^{-1}; TEM of typical samples shown in **Figure 4B** were encapsulated in ZIF at ambient conditions mixing the proteoliposome complexes with a solution of MIM and zinc acetate dihydrate using M-buffer as solvent. Crystals were harvested by centrifugation after 18 h of aging at RT, washed with ultrapure water and allowed to dry at RT for 12 h (**Figure 4C**). SDS-PAGE gel densitometry revealed protein recovery after exfoliation with no detectable traces of protein in the supernatants (**Figure S11 A**). In the presence of sodium chloride, TCEP or DTT, and MOPs the crystal morphology appears as aggregates of star-like shape chunks (**Figures S11 B-H)** of ZIF-L. The encapsulation and exfoliation process, which were optimized in the prior two studies, was very straight forward for proteoliposome assemblies to generate IroTPL@ZIF and CopA-PL@ZIF biocomposites. Following exfoliation, we found the proteoliposome size and shape were not altered compared to freshly extruded proteoliposomes by TEM and DLS analyses, even after heat exposures, regardless of the ZIF formulation utilized for immobilization (**Figure 4E**, **Figure S12 and Table S3 and S4**).

In addition to the size and morphology preservation, activity assays performed on the ZIF immobilized CopA proteoliposomes confirmed that the MOF shell thermally enhances these delicate systems enabling them to

resist temperatures that would otherwise promote loss of function (**Figures 4 F-I**). Indeed, proteoliposome formulations of CopA are so thermally unstable they lose 90% of their catalytic activity in 48 h at 4 °C (**Figure S13**).

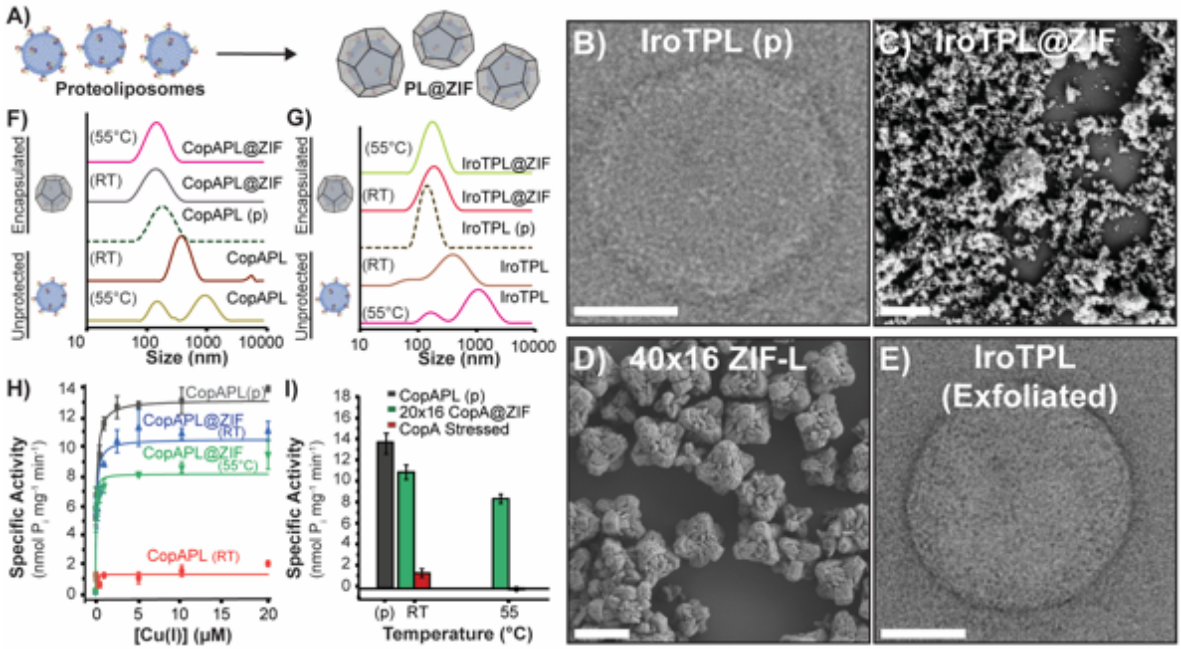

Figure 4. Characterization of proteoliposome@ZIF bio-composites. A) Biomolecular nucleation of CopA-PL and IroTPL in ZIF-L. B) TEM micrograph of pristine IroT containing proteoliposomes. (Scale bar= 50 nm) C) SEM micrograph of IroT-PL@ZIF bio-composites.(Scale bar= 1 μm). D) SEM micrograph of ZIF-L control. (Scale bar= 1 μm). E) TEM micrograph of a recovered fully functional IroT containing proteoliposome upon complete exfoliation. (Scale bar= 100 nm). DLS of F) 20×16 CopA-PL@ZIF bio-composites after thermal stressing followed by exfoliation compared to controls and G) 40×16 IroTPL@ZIF bio-composites after temperature stressing followed by exfoliation compared to controls. H) Specific activity of 20×16 CopA-PL@ZIF bio-composites stressed at RT and 55 °C. I) Comparison of maximal specific activity at saturating Cu^+ concentration of 20×16 CopA-PL@ZIF bio-composites stressed at RT and 55 °C to the non-encapsulated and stressed CopA-PL

To demonstrate that the encapsulated proteoliposomes not only resist prolonged periods of no refrigeration but also enhances stability towards physical/mechanical stressors, prepared PL@ZIF samples were shipped across America in a padded envelope through the United States Postal Service. PL@ZIF bio-composites in water were placed in a standard cushioned mailer and shipped across the United States, from Dallas, Texas to Rhode Island and back again. They were then left at room temperature for two months following shutdown of our laboratories during the 2020 SARS-CoV-2 pandemic. By the time we had opened the package, the water had completely evaporated. Nonetheless, after exfoliation, the catalytic activity and liposome morphology were similar to the pristine counterparts (**Figure S14**) in contrast to controls, which we know degrade within a day at room temperature or two days under refrigerated conditions.

Conclusion

Lipid bilayers are the core building unit of cell membranes, which serve as the main line of action between the outside and the inside environments of the cells and organelles. Given their structural complexity, researchers have been motivated to develop simpler model systems to understand the molecular processes associated with cellular membrane dynamics and investigate protein-mediated solute translocation across lipid bilayers. Proteoliposomes are a powerful tool that mimic cellular membranes. By virtue of tuning the vesicle size and the lipid and protein composition, proteoliposomes have become instrumental to the study both prokaryotic and complex eukaryotic cell membranes, and

proteins embedded into them, including transmembrane transporter proteins. Despite their utility, proteoliposomes are delicate systems that require unique conditions to maintain their functionality that have long imposed obstacles for their handling/transport and hindering their usefulness for the better understanding of the *modus operandi* of transmembrane proteins. Taking advantage of the high thermal and aqueous stabilities of ZIF-L, blank liposomes, detergent-solubilized proteins, and proteoliposome complexes no longer require constant refrigeration and repeated extrusion to maintain their intrinsic structure, monodispersity and functionality over long incubation times. Further, we show that immobilization in ZIF-L enables the as-prepared bio-composites to be exposed to chemical denaturants and temperatures above their lipid bilayer phase transition without structural and/or functional changes. Finally, we have shown that biomolecular nucleation is an effective process to preserve supramolecular membrane protein-lipid bilayer assemblies against conditions that, without encapsulation, would easily impair their structural and functional integrity.

References

1. Ma, Z., Jacobsen, F.E. & Giedroc, D.P. Coordination chemistry of bacterial metal transport and sensing. *Chem. Rev.* **109**, 4644-4681 (2009).
2. Giacomini, K.M. et al. Membrane transporters in drug development. *Nat. Rev. Drug discovery* **9**, 215-236 (2010).
3. Busch, W. & Saier, M.H., Jr. The transporter classification (TC) system, 2002. *Crit. Rev. Biochem. Mol. Biol.* **37**, 287-337 (2002).
4. Saier, M.H., Jr et al. The transporter classification database (TCDB): recent advances. *Nucleic Acids Res.* **44**, D372-D379 (2015).
5. Geertsma, E.R., Nik Mahmood, N.A.B., Schuurman-Wolters, G.K. & Poolman, B. Membrane reconstitution of ABC transporters and assays of translocator function. *Nat. Protoc.* **3**, 256-266 (2008).
6. Scalise, M., Pochini, L., Giangregorio, N., Tonazzi, A. & Indiveri, C. Proteoliposomes as tool for assaying membrane transporter functions and interactions with xenobiotics. *Pharmaceutics* **5**, 472-497 (2013).
7. Panganiban, B. et al. Random heteropolymers preserve protein function in foreign environments. *Science (New York, N.Y.)* **359**, 1239-1243 (2018).
8. Fiori, M.C. et al. Extraction and reconstitution of membrane proteins into lipid nanodiscs encased by zwitterionic styrene-maleic amide copolymers. *Sci. Rep.* **10**, 9940 (2020).
9. Lu, K., Aung, T., Guo, N., Weichselbaum, R. & Lin, W. Nanoscale metal–organic frameworks for therapeutic, imaging, and sensing applications. *Adv. Mater.* **30**, 1707634 (2018).
10. Yuan, S. et al. Stable metal–organic frameworks: design, synthesis, and applications. *Adv. Mater.* **30**, 1704303 (2018).
11. Riccò, R. et al. Metal–organic frameworks for cell and virus biology: a perspective. *ACS Nano* **12**, 13-23 (2018).
12. Chen, B., Yang, Z., Zhu, Y. & Xia, Y. Zeolitic imidazolate framework materials: recent progress in synthesis and applications. *J. Mater. Chem. A* **2**, 16811-16831 (2014).
13. Pan, Y. & Lai, Z. Sharp separation of C2/C3 hydrocarbon mixtures by zeolitic imidazolate framework-8 (ZIF-8) membranes synthesized in aqueous solutions. *Chem. Commun.* **47**, 10275-10277 (2011).
14. Li, B., Wen, H.-M., Zhou, W. & Chen, B. Porous metal–organic frameworks for gas storage and separation: what, how, and why? *J. Phys. Chem. Lett.* **5**, 3468-3479 (2014).
15. Ellis, J.E. et al. Growth of ZIF-8 on molecularly ordered 2-methylimidazole/single-walled carbon nanotubes to form highly porous, electrically conductive composites. *Chem. Sci.* **10**, 737-742 (2019).
16. Wang, Q. & Astruc, D. State of the art and prospects in metal–organic framework (MOF)-based and MOF-derived nanocatalysis. *Chem. Rev.* **120**, 1438-1511 (2020).
17. Pascanu, V., González Miera, G., Inge, A.K. & Martín-Matute, B. Metal–organic frameworks as catalysts for organic synthesis: a critical perspective. *J. Am. Chem. Soc.* **141**, 7223-7234 (2019).
18. Li, S. et al. Hierarchical porous carbon arising from metal–organic framework-encapsulated bacteria and its energy storage potential. *ACS Appl. Mater. Interfaces* **12**, 11884-11889 (2020).
19. Chen, Y., Li, P., Modica, J.A., Drout, R.J. & Farha, O.K. Acid-resistant mesoporous metal–organic framework toward oral insulin delivery: protein encapsulation, protection, and release. *J. Am. Chem. Soc.* **140**, 5678-5681 (2018).
20. Wang, C. et al. Metal–organic framework encapsulation for biospecimen preservation. *Chem. Mater.* **30**, 1291-1300 (2018).
21. Lykourinou, V. et al. Immobilization of MP-11 into a mesoporous metal–organic framework, MP-11@mesoMOF: a new platform for enzymatic catalysis. *J. Am. Chem. Soc.* **133**, 10382-10385 (2011).
22. Eddaoudi, M., Sava, D.F., Eubank, J.F., Adil, K. & Guillerm, V. Zeolite-like metal–organic frameworks (ZMOFs): design, synthesis, and properties. *Chem. Soc. Rev.* **44**, 228-249 (2015).
23. Liang, W. et al. Control of structure topology and spatial distribution of biomacromolecules in protein@ZIF-8 biocomposites. *Chem. Mater.* **30**, 1069-1077 (2018).
24. Park, K.S. et al. Exceptional chemical and thermal stability of zeolitic imidazolate frameworks. *Proc. Natl. Acad. Sci. U. S. A.* **103**, 10186-10191 (2006).
25. Liang, K., Coghlan, C.J., Bell, S.G., Doonan, C. & Falcaro, P. Enzyme encapsulation in zeolitic imidazolate frameworks: a comparison between controlled co-precipitation and biomimetic mineralisation. *Chem. Commun.* **52**, 473-476 (2016).
26. Liang, K. et al. Biomimetic mineralization of metal-organic frameworks as protective coatings for biomacromolecules. *Nat. Commun.* **6**, 7240 (2015).
27. Wang, C. et al. Metal-organic framework encapsulation preserves the bioactivity of protein therapeutics. *Adv. Healthcare Mater.* **7**, 1800950 (2018).
28. Luzuriaga, M.A. et al. Enhanced stability and controlled delivery of MOF-encapsulated vaccines and their immunogenic response in vivo. *ACS Appl. Mater. Interfaces* **11**, 9740-9746 (2019).
29. Luzuriaga, M.A. et al. ZIF-8 degrades in cell media, serum, and some—but not all—common laboratory buffers. *Supramol. Chem.* **31**, 485-490 (2019).

30. Li, S. et al. Investigation of controlled growth of metal–organic frameworks on anisotropic virus particles. *ACS Appl. Mater. Interfaces* **10**, 18161-18169 (2018).
31. Luzuriaga, M.A. et al. A whole cell metal-organic framework encapsulated vaccine against septicemic UPEC infection. *bioRxiv*, 2020.2006.2014.148452 (2020).
32. Newton, H.J., Ang, D.K.Y., van Driel, I.R. & Hartland, E.L. Molecular pathogenesis of infections caused by Legionella pneumophila. *Clin. Microbiol. Rev.* **23**, 274-298 (2010).
33. Ward, S.K., Abomoelak, B., Hoye, E.A., Steinberg, H. & Talaat, A.M. CtpV: a putative copper exporter required for full virulence of Mycobacterium tuberculosis. *Mol. Microbiol.* **77**, 1096-1110 (2010).
34. Ren, F. et al. X-ray structures of the high-affinity copper transporter Ctr1. *Nat. Commun.* **10**, 1386 (2019).
35. Andersson, M. et al. Copper-transporting P-type ATPases use a unique ion-release pathway. *Nat Struct Mol Biol* **21**, 43-48 (2014).
36. Smith, A.T., Barupala, D., Stemmler, T.L. & Rosenzweig, A.C. A new metal binding domain involved in cadmium, cobalt and zinc transport. *Nat. Chem. Biol.* **11**, 678-684 (2015).
37. Li, S. et al. Template-directed synthesis of porous and protective core–shell bionanoparticles. *Angew. Chem. Int. Ed.* **55**, 10691-10696 (2016).
38. Maddigan, N.K. et al. Protein surface functionalisation as a general strategy for facilitating biomimetic mineralisation of ZIF-8. *Chem. Sci.* **9**, 4217-4223 (2018).
39. Low, Z.-X et al. Crystal transformation in zeolitic-imidazolate framework. *Cryst. Growth Des*. **14,** 6589-6598 (2014).
40. Nasir, A.M., Md Nordin, N.A.H., GoH, P.S. & Ismail, A.F. Application of two-dimensional leaf-shaped zeolitic imidazolate framework (2D ZIF-L) as arsenite absorbent: Kinetic, isotherm and mechanism. *J. Mol. Liq.* **250,** 269-277 (2018).
41. Chen,R. et al. A two-dimensional zeolitic imidazolate framework with a cusion-shaped cavity for CO_2 adsorption. *Chem. Commun.* **49**, 9500-9502 (2013).41.
42. Carraro, F. et al. Continuous-flow synthesis of ZIF-8 biocomposites with tunable particle size. *Angew. Chem. Int. Ed.* **59,** 8123-8127 (2020).
43. Liang,W. et al. Enhanced activity of enzymes encapsulated in hydrophilic metal-organic frameworks. *J. Am. Chem. Soc.* **141,** 2348-2355 (2019).
44. Ogata, A.F. et al. Direct observation of amorphous precursor phases in the nucleation of protein-metal-organic frameworks. *J. Am. Chem. Soc.* **142,** 1433-1442 (2020).
45. Astria, E. et al. Carohydrates@MOFs. *Mater. Horiz.* **6,** 969-977 (2019).
46. Isaac, D.T., Laguna, R.K., Valtz, N. & Isberg, R.R. MavN is a Legionella pneumophila vacuole-associated protein required for efficient iron acquisition during intracellular growth. *Proc. Natl. Acad. Sci. U. S. A.* **112**, E5208-E5217 (2015).
47. Portier, E. et al. IroT/mavN, a new iron-regulated gene involved in Legionella pneumophila virulence against amoebae and macrophages. *Environ. Microbiol.* **17**, 1338-1350 (2015).
48. Christenson, E.T. et al. The iron-regulated vacuolar Legionella pneumophila MavN protein is a transition-metal transporter. *Proc. Natl. Acad. Sci. U. S. A.* **116**, 17775-17785 (2019).
49. Abeyrathna, S.S. et al. IroT/MavN is a Legionella transmembrane Fe(II) transporter: metal selectivity and translocation kinetics revealed by in vitro real-time transport. *Biochemistry* **58**, 4337-4342 (2019).
50. Wijekoon, C.J.K. et al. Copper ATPase CopA from Escherichia coli: quantitative correlation between ATPase activity and vectorial copper Transport. *J. Am. Chem. Soc.* **139**, 4266-4269 (2017).
51. Argüello, J.M., Patel, S.J. & Quintana, J. Bacterial Cu+-ATPases: models for molecular structure–function studies. *Metallomics* **8**, 906-914 (2016).
52. Abeyrathna, N., Abeyrathna, S., Morgan, M.T., Fahrni, C.J. & Meloni, G. Transmembrane Cu(i) P-type ATPase pumps are electrogenic uniporters. *Dalton Tran.* (2020).
53. Lutsenko, S., Barnes, N.L., Bartee, M.Y. & Dmitriev, O.Y. Function and regulation of human copper-transporting ATPases. *Physiol. Rev*. **87**, 1011-1046 (2007).
54. Gourdon, P. et al. Crystal structure of copper-transporting PIB-type ATPase. *Nature* **475**, 59-64 (2011).
55. Alquethamy, S.F. et al. The Role of the CopA Copper Efflux System in Acinetobacter baumannii Virulence. *Int. J. Mol. Sci.* **20,** 575 (2019).

Acknowledgements
This project was partially funded by The University of Texas at Dallas Office of Research through the SPIRe grant program. J.J.G. thanks the National Science Foundation (CAREER DMR-1654405 and DMR-2003534) and the Welch Foundation (AT-1989- 20190330). The work in G.M. laboratory was supported by the Robert A. Welch Foundation (Grant: AT-1935-20170325 to G.M) and by the National Institute of General Medical Sciences of the National Institutes of Health under Award Number R35GM128704 (to G.M.). The content is solely the responsibility of the authors and does not necessarily represent the official views of the National Institutes of Health. R.A.S acknowledges support from the Army Research Laboratory (W911NF-18-2-0035). A.D.S acknowledges Consejo Nacional de Ciencia y Tecnología (National Council for Science and Technology) of Mexico for a doctoral fellowship. FC and PF acknowledge European Union's Horizon 2020 Programme (FP/2104-2020)/ERC Grant Agreement no. 771834 POPCRYSTAL. TU Graz for the Lead Project (LP-03), and the CERIC-ERIC Consortium for the access to experimental facilities and financial support.

Author Contribution
[§]F.C.H., S.S.A, and N.S.A contributed equally to this manuscript. Primary manuscript writing and editing was done by F.C.H. G.M. and J.J.G. Blank liposome, IroT, and IroTPL encapsulation, stressing, was done by F.C.H. IroT

expression, purification, proteoliposome preparation, SECs of IroT/IroTPL were performed by S.S.A. CopA expression purification, proteoliposome preparation, and ATPase activity assays were done by N.S.A. CopA/CopA-PL encapsulation and stressing were done by Y.H.W. SDS was done by F.C.H, S.S.A., N.S.A., and Y.H.W. DLS was done by F.C.H., S.S.A, and Y.H.W. TEMs were taken by O.R.B. SEMs were taken by M.A.L. and O.R.B. PXRDs were done by F.C.H and M.A.L. TGA was done by A.D.S. Nitrogen sorption and BET analysis were done by S.D.D. The synthesis of Lp@ZIF was independently verified and SAXS/WAXS experiments were performed by F.C., H.A, and P.F.; SAXS/WAXS data was interpreted by F.C., H.A, and M. F. Funding was raised by R.A.S, G.M. and J.J.G.

Competing Interest
The authors declare no competing interest